



Direct-Write Planar Microultracapacitors by Laser Engineering

Craig B. Arnold,^{a,z} Ryan C. Wartena,^{b,*} Karen E. Swider-Lyons,^{b,*}
and Alberto Pique^a

^aMaterials Science and Technology Division, ^bChemistry Division Naval Research Laboratory, Washington, District of Columbia 20375, USA

We have successfully employed laser direct write and micromachining to fabricate high capacity hydrous ruthenium oxide (RuO_xH_y or $\text{RuO}_2 \cdot x\text{H}_2\text{O}$) microultracapacitors. A laser direct-write process is used to deposit uniform pads of $\text{RuO}_2 \cdot 0.5\text{H}_2\text{O}$ in sulfuric acid under ambient temperature and atmospheric conditions. Ultraviolet laser micromachining is used to tailor the shape and size of the deposited material into planar electrodes. The specific capacitance of the laser-deposited materials is comparable to reported values of ~ 720 F/g. The microultracapacitors demonstrate linear charge and discharge behavior at currents below 1 mA, as expected for an ideal capacitor. By studying the charge storage and power output as a function of discharge current, the power can be successfully modeled assuming only simple ohmic losses. Parallel and series combinations of these microultracapacitor cells provide the expected addition of capacitance. Maximum discharge currents of 50 mA are applied to two cells in parallel without damage to the microultracapacitor cells. The microultracapacitors exhibit high specific power and specific energy with over 1100 mW/g at approximately 9 mWhr/g for an 80 μm cell with a footprint of 2 mm^2 and a thickness of 15 μm .

© 2003 The Electrochemical Society. [DOI: 10.1149/1.1563650] All rights reserved.

Manuscript submitted May 30, 2002; revised manuscript received November 2, 2002. Available electronically March 20, 2003.

High capacitance electrochemical capacitors (ultracapacitors or supercapacitors) are recognized as a key component for many energy storage systems because of their ability to deliver pulsed power and provide load leveling.¹⁻³ In the last decade, ultracapacitors have gained widespread attention in large commercial applications, such as electric or hybrid powered vehicles and power backup systems. The need for high power pulsed energy is also critical for the operation of autonomous microelectronic systems such as microsensors or microelectromechanical systems.⁴ The size constraints of such microdevices require power sources with high energy and power per unit mass and/or volume in a package of commensurate size. These requirements are unable to be met by the current generation of microbatteries or micro-fuel cells alone.^{4,5} Thus microultracapacitors provide a solution for micro-power generation through combination with high energy storage sources to supply the desired energy and power for these microdevices.⁶

Hydrous ruthenium oxide ($\text{RuO}_2 \cdot x\text{H}_2\text{O}$) is an ideal electrode material for a microultracapacitor because of its high specific capacitance (720 F/g for $x = 0.5$).⁷ The rapid double insertion and release of protons and electrons in the RuO_2 leads to a large pseudocapacitance effect, which, in combination with a high specific surface area, leads to the high amounts of charge storage by the material.⁷⁻⁹ This pseudocapacitance effect is enhanced by the presence of structural water in the lattice which provides nanostructured percolation pathways for proton conduction into the bulk of the material.¹⁰ The capacitance of the $\text{RuO}_2 \cdot x\text{H}_2\text{O}$ sensitively depends on the processing temperature through the loss of structural water, and it is maximized when the hydrous material is heated to ~ 150 - 170°C to yield a chemical formula of $\text{RuO}_2 \cdot 0.5\text{H}_2\text{O}$.^{7,10,11}

High specific surface area requirements, processing temperature limitations, and the presence of water in the porous oxide structure, have made the deposition of $\text{RuO}_2 \cdot x\text{H}_2\text{O}$ films incompatible with standard vacuum techniques such as physical or chemical vapor deposition for thin film growth. Other thin-film techniques such as sol-gel techniques¹² or electrostatic spray deposition¹³ are compatible with the material constraints, but require multiple processing steps including additional lithography to produce the three-dimensional structures required for making microultracapacitors.

We overcome these difficulties associated with the deposition of hydrous ruthenium oxide microultracapacitors by using a laser direct-write process.^{14,15} The laser process allows us to deposit and

modify structures and patterns of the material in three dimensions without the need for additional *ex situ* processing steps. In this technique, an "ink" composed of a sacrificial liquid matrix (transfer vehicle) and the material to be deposited (passenger material) is laser forward transferred to a substrate. The relative compositions of passenger material and transfer vehicle can be modified easily and can include additives to affect the as-deposited material properties. The liquid component of the ink allows the material to flow and achieve a uniform, pinhole-free surface.¹⁶ Films of hydrous materials are produced with the desired morphological properties, and shaped into the appropriate electrode configurations using UV laser micromachining in the same apparatus, without the need for additional high temperature or lithographic processing steps.¹⁷

A distinct advantage of the laser direct-write technique is the ability to operate under ambient conditions to deposit inks composed of $\text{RuO}_2 \cdot 0.5\text{H}_2\text{O}$ (passenger) and liquid sulfuric acid (vehicle).¹⁸ The use of the liquid sulfuric acid electrolyte enables higher proton conductivity in the electrolyte and enhances ultracapacitor properties.¹⁹ The ability to deposit the electrolyte with the electrode material is an attractive aspect of the laser transfer process that is not compatible with many other thin film deposition techniques.

In this paper, we demonstrate the fabrication of planar microultracapacitors of hydrous ruthenium oxide ($\text{RuO}_2 \cdot 0.5\text{H}_2\text{O}$) using the laser direct-write technique. We examine their electrochemical charge storage properties and study their energy and power output as a function of discharge current. A simple ohmic loss model is used to describe the observed power dependence. The parallel and series combinations of cells are shown to add as expected and enable us to attain higher discharge currents (up to 50 mA) and higher potentials (up to 2 V) in comparison to single-cell measurements.

Experimental

Hydrous ruthenium oxide planar microultracapacitors are deposited using a laser direct-write technique, details of which have been described in previous work.^{14,15} Figure 1 shows a schematic of the experimental approach. Commercially available hydrous ruthenium oxide power (Alfa-Aesar) is oven heated to 150°C for 18 h to yield a material with the desired water content of 0.5 mol H_2O per mol RuO_2 for optimal charge storage.^{7,20} The dry powder is combined with 5 M sulfuric acid to form the ink, which is spread with a no. 6 wire coater on a borosilicate plate to form a coating approximately 5 μm thick (Fig. 1a). The $\text{RuO}_2 \cdot 0.5\text{H}_2\text{O} + \text{H}_2\text{SO}_4$ ink is irradiated through the back of the borosilicate plate using a frequency-tripled Nd:YAG laser ($\lambda = 355$ nm) to induce the forward transfer of material to a substrate 100 μm below the ribbon.

* Electrochemical Society Active Member.

^z E-mail: craig.arnold@nrl.navy.mil

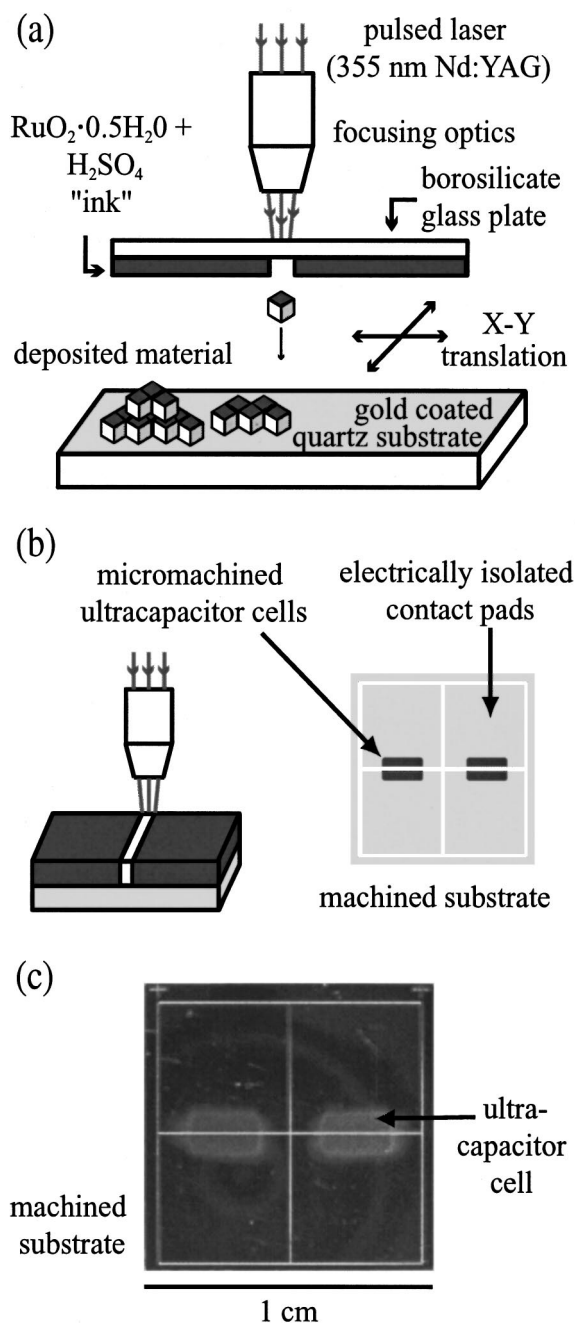


Figure 1. Experimental setup showing the configuration for (a) laser direct-write and (b) micromachining to produce a planar $\text{RuO}_2 \cdot 0.5\text{H}_2\text{O}$ microultracapacitor. (c) Picture of laser machined planar microultracapacitors on a gold-coated quartz substrate.

The substrate is a 1×1 cm gold-coated quartz wafer that has been laser machined with a "window pane" structure to electrically isolate four current collector pads (Fig. 1b). Hydrous ruthenium oxide films, approximately 1×2 mm \times $15 \mu\text{m}$ thick, are deposited across the machined groove in the gold. A $20 \mu\text{m}$ wide line is then UV laser machined across the film to establish a symmetric planar ultracapacitor with two identical 0.5×2 mm \times $15 \mu\text{m}$ electrodes. Two such ultracapacitors are deposited on each substrate, as shown in Fig. 1c. For the cyclic voltammetry (CV) experiments, a single 2.3×2.3 mm $\text{RuO}_2 \cdot 0.5\text{H}_2\text{O}$ pad is deposited on graphite foil and no micromachining is performed.

We use white light interferometry (Zygo New View 5022) to determine the actual surface morphology as well as the volume of

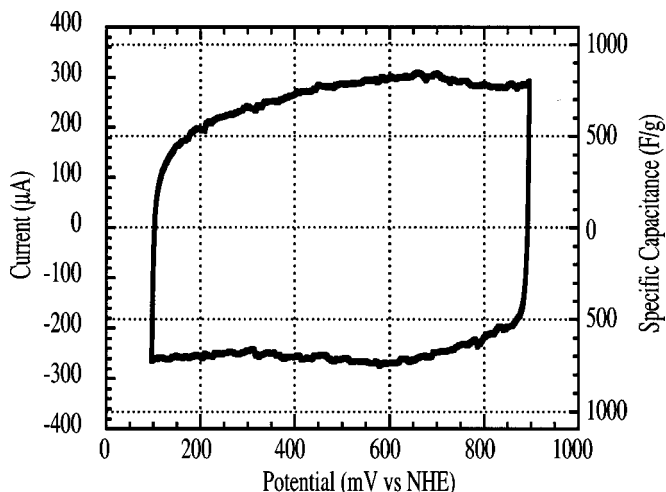


Figure 2. CV of laser transferred $\text{RuO}_2 \cdot 0.5\text{H}_2\text{O}$ electrode material on graphite foil in $0.5 \text{ M H}_2\text{SO}_4$ at a 5 mV/s scan rate. The right hand axis shows the converted values of current to specific capacitance using the mass of active material in the sample ($70 \mu\text{g}$). The electrode area of this sample is 5 mm^2 .

the ultracapacitor cells, which is approximately 3×10^{-5} mL per ultracapacitor cell. The mass of the ultracapacitors is measured on a microbalance (Sartorius M2P) where the typical mass, following deposition and micromachining, is approximately $100 \mu\text{g}$. For this measurement we include the mass of the active material as well as the transferred H_2SO_4 , but do not include the mass of the substrate or gold current collectors. Due to differences in the thickness of the ink coating on the glass plate from run to run, the actual values for volume and mass may vary by as much as 20% for different cells.

To prevent delamination of the electrodes, a Nafion film is formed on top of the $\text{RuO}_2 \cdot 0.5\text{H}_2\text{O}$ by drop casting a 5% ionomer solution (Ion Power, Liquion 1100) on the deposited material and air drying. The $\text{RuO}_2 \cdot 0.5\text{H}_2\text{O}$ -Nafion ensemble is then covered by a droplet of $0.5 \text{ M H}_2\text{SO}_4$ solution and is allowed 5-10 min to equilibrate before acquiring data. Electrochemical evaluation of capacitance through CV and chronopotentiometry is carried out using a potentiostat (EG&G PAR model 263) connected to a probe station. Multiple chronopotentiometry steps are used to charge and discharge the ultracapacitors between 0 and 1 V in a two-electrode configuration. All cells tested for this work are charged at a constant current of $50 \mu\text{A}$. CV is performed in $0.5 \text{ M H}_2\text{SO}_4$ over the potential range of 100-900 mV vs. a normal hydrogen electrode (NHE) at various scan rates in a three electrode configuration using a Pd/H reference electrode and a platinum counterelectrode. All potentials reported in this paper are relative to NHE.

Results and Discussion

Electrochemical characterization of deposited material.—The voltammetric behavior of a laser transferred electrode coated with Nafion on graphite foil is shown in Fig. 2 for a scan rate of 5 mV/s over the potential window of 100-900 mV in $0.5 \text{ M H}_2\text{SO}_4$ at ambient temperatures. The open circuit potentials (OCPs) for these samples range between 750 and 850 mV. Voltammetry curves show nearly constant current behavior over the potential window, indicative of ideal capacitive behavior as previously reported for the hydrous ruthenium oxide system.^{7,21} The specific capacitance of the electrode material is calculated from $c = I/mv$, where v is the voltage scan rate, I is the measured current, and m is the mass of active material only. For this particular sample, the mass is $70 \mu\text{g}$ with an electrode area of 5 mm^2 . The average value of 720 F/g , obtained by averaging the current over the entire voltage window, is consistent with the reported literature values for $\text{RuO}_2 \cdot 0.5\text{H}_2\text{O}$ deposited

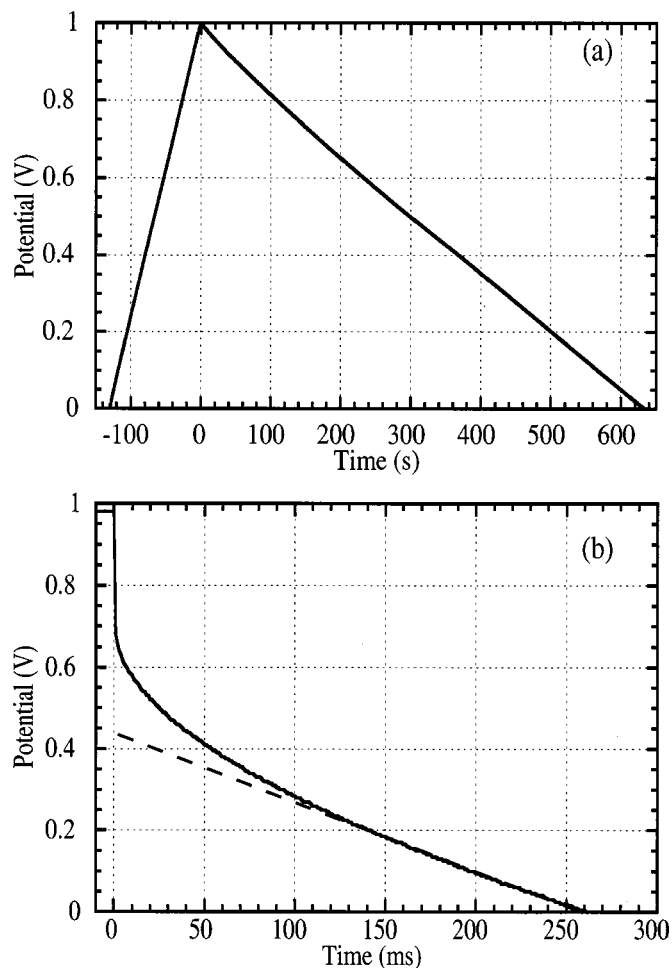


Figure 3. Chronopotentiometry data from single microultracapacitor cell charged at 50 μA and discharged at (a) 10 μA and (b) 5 mA. The dashed line in (b) represents an extrapolation of the linear discharge regime.

by other techniques.^{7,13} These results indicate that the active $\text{RuO}_2 \cdot 0.5\text{H}_2\text{O}$ material is not significantly affected by our laser deposition technique.

Electrochemical characterization of ultracapacitor cell.—The chronopotentiometry of a single microultracapacitor cell is shown by a solid line in Fig. 3a for a constant charging current of 50 μA and a discharge current of 10 μA . Linear behavior is observed during both charging and discharging cycles, thereby demonstrating the expected behavior of an ideal capacitor. Under these conditions, the average time for charging is $\Delta t_c = 130 \pm 2$ s corresponding to a calculated capacitance of $C_c = 6.5 \pm 0.1$ mF, where the uncertainty is determined by statistical analysis of 50 charging/discharging cycles. The capacitance calculated from the discharge portion of the chronopotentiometry gives similar values of capacitance with $\Delta t_d = 640 \pm 5$ s and $C_d = 6.4 \pm 0.05$ mF. The specific capacitance is determined by normalizing the actual capacitance by the experimentally measured mass of the deposited material (active material and electrolyte), 80 ± 2 μg , yielding $c_c = 80 \pm 2.5$ F/g and $c_d = 78 \pm 2.3$ F/g. The values for specific capacitance may vary by as much as 5% from cell to cell.

At high discharge currents (above 1 mA), there is a transient, nonlinear behavior due to resistive losses in the system. Figure 3b shows the discharge of a microultracapacitor cell at 5 mA for a total discharge time of 260 ± 2 ms. A single cell can be discharged at currents up to 10 mA without irreversible damage. The total resistance of the cell is estimated by extrapolating the linear discharge

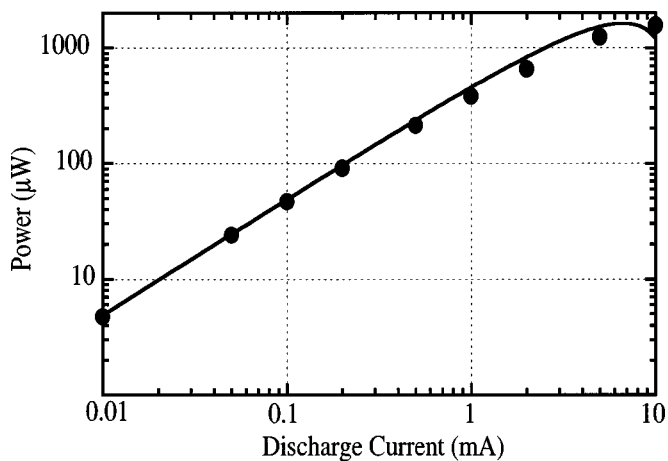


Figure 4. Power as a function of discharge current for a single microultracapacitor cell obtained from chronopotentiometry measurements using Eq. 1 over the range of 0–1 V. The fit corresponds to Eq. 2 using the measured steady-state cell resistance of 75 Ω .

region to $t = 0$, as shown by a dashed line in Fig. 3b.²² We find a resistance, $R = 75$ Ω at a 10 mA discharge current. The measured resistance is primarily due to the resistivity of the electrolyte which is 3–4 orders of magnitude higher than that of the metallicly conductive $\text{RuO}_2 \cdot 0.5\text{H}_2\text{O}$ ($\rho \sim 1\text{--}10$ Ω cm vs. 3.23 m Ω cm). A simple calculation of the electrolyte resistance based on our electrode geometry (neglecting porosity) yields a resistance of 10–100 Ω which is consistent with our measured value. The resistance capacitance (RC) time constant of the microultracapacitor cell is approximately 0.5 s.

The relationship between power output and discharge current demonstrates the importance of internal cell resistance and is shown in Fig. 4. The power of the microultracapacitor cells is calculated from the area under the discharge curve between 0 and 1 V using the equation

$$P = \frac{I \int V dt}{\Delta t} \quad [1]$$

where Δt is the total discharge time which depends on the discharge current, I . The power increases linearly for currents below 1 mA as expected for a capacitor. At higher currents, the power is no longer proportional to the discharge current because of contributions of the polarization losses in the system. The full treatment of total polarization losses and how they affect the power in such a capacitor system has been discussed extensively in the literature (for example, Ref. 23–25).

We assume that the polarization losses are due primarily to ohmic contributions in this current range and neglect the contribution of activation (Tafel) and concentration polarizations. We can then express the power as

$$P = \frac{1}{2} I (V_0 - IR) \quad [2]$$

where V_0 is the reversible potential for the system. Figure 4 shows the parameter-free fit of the data using Eq. 2 with the values V_0 and R as measured in our experiment. There is excellent agreement between the calculated and experimental results, even at higher currents, which demonstrates that the ohmic term dominates the polarization losses in our microultracapacitors at the currents examined in this experiment. This result should enable us to make predictions for the power dependence as the cell resistance is changed by modifying the electrode geometry.

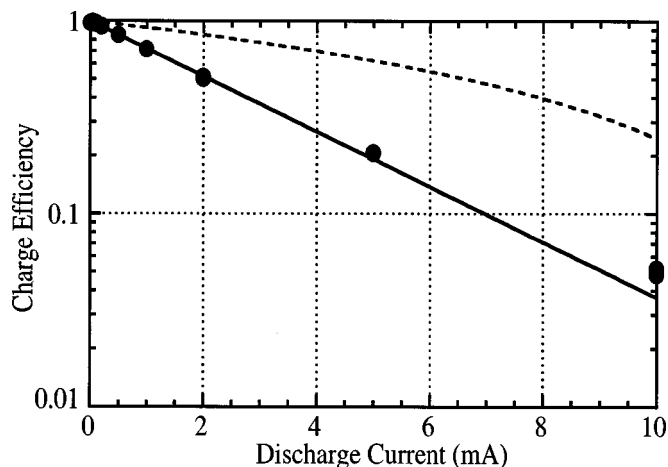


Figure 5. Charge efficiency, $\epsilon \equiv Q_{\text{out}}/Q_{\text{in}}$, as a function of the discharge current. The solid line represents a fit to a simple decaying exponential function, $\epsilon = \exp(-\beta I)$, with fitting parameter $\beta = 0.33 \text{ mA}^{-1}$. The dashed line represents the expected behavior assuming only ohmic losses in the system, $\epsilon = 1 - IR/V_0$, using the values from Fig. 4.

The charge efficiency of the microultracapacitor as a function of discharge current is shown in Fig. 5. We define the charge efficiency, ϵ , as the amount of charge extracted during discharge normalized by the amount of charge added to the system during charging, $\epsilon \equiv Q_{\text{out}}/Q_{\text{in}}$. The data appears to decay as a simple exponential with 90% efficiency occurring for a current of approximately 300 μA . We use β as a free fitting parameter in the equation, $\epsilon = \exp(-\beta I)$ to generate the fit for $\beta = 0.33 \text{ mA}^{-1}$ shown with a solid line in the figure.

A decrease in charge efficiency with increasing current is expected due to polarization losses. However, the dashed line in Fig. 5 shows this behavior if we assume only ohmic losses in the system as in Eq. 2. Based on theoretical considerations, the addition of simple concentration or activation polarizations to the total overpotential would not significantly improve the fit as they provide terms of order $\ln(I)$ instead of the exponential dependence observed in our experiment. A similar behavior has been experimentally observed by others^{21,26} and was suggested to be related to the decrease in electrode capacitance as a function of increasing voltage scan rate.

Parallel and series combinations.—We examine the combination of our microultracapacitor cells in parallel and series configurations to determine their ability to supply higher currents and voltages. Figure 6 shows the charge and discharge curves at currents of 50 and 10 μA , respectively, for series and parallel configurations of two cells. The series configuration is charged to 2 V while the parallel configuration is charged to 1 V. In both cases, the discharge behavior remains nearly linear. The capacitance for the combinations are $3.5 \pm 0.06 \text{ mF}$ in series and $14.1 \pm 0.25 \text{ mF}$ in parallel, averaged over 50 cycles. In comparison, the capacitance of the individual capacitors are 6.5 and 8.3 mF with the calculated series and parallel combinations of 3.65 and 14.8 mF, respectively. Our measured capacitances for series and parallel combinations exhibit the proper addition of capacitance (within 5%) as compared to the theoretical combination of the individual cells.

Figure 7 shows the power as a function of the discharge current for the individual cell as well as that for the series and parallel combinations of two similar cells. In this plot, the power is calculated between 0 and 1 V for the single cell and the parallel combination and between 0 and 2 V for the series combination. As for the single cell, the power increases with current until the polarization losses cause the power to diverge from linear behavior and eventually decrease as a function of current. For the two cells in parallel, there is less of a deviation from linear behavior at high currents

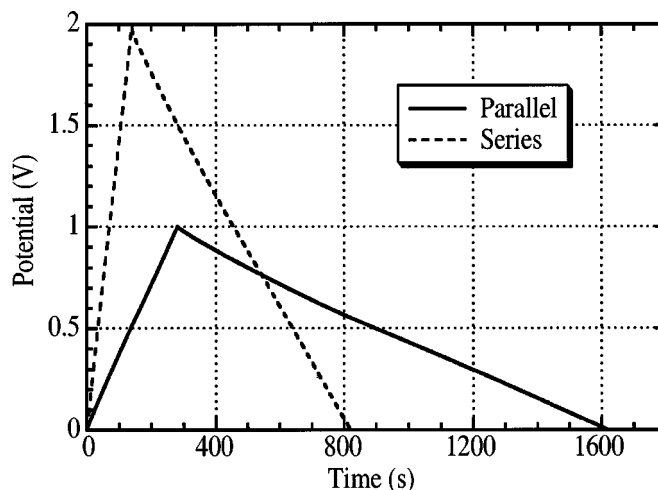


Figure 6. Chronopotentiometry data from (solid line) parallel and (dotted line) series microultracapacitor cells charged at 50 μA and discharged at 10 μA .

because the reduced resistance decreases the ohmic losses. The correspondingly smaller initial IR drop enables the parallel combination of cells to be discharged at currents as high as 50 mA without damage. In the case of two cells in series, the power is approximately twice that of a single cell, because of the doubled potential. The deviation from linear behavior in power occurs at discharge currents $\sim 2 \text{ mA}$ and at 20 mA the ohmic losses cause a significant decrease in the available power.

Specific power and specific energy.—The specific power is compared to the specific energy in Fig. 8 for our microultracapacitor cells. We have normalized the power and energy by the mass of the deposited material ($\text{RuO}_2 \cdot 0.5\text{H}_2\text{O}$ plus transferred electrolyte). The masses of the substrate, encapsulation, and additional electrolyte are not included in this calculation. Such an accounting of mass is justified for these microultracapacitors because, under typical applications, they would be directly integrated on the substrate of a completed device (such as a microsensor or transmitter).⁶

The specific power increases with decreasing specific energy as predicted by others.^{27,28} For a single cell of mass 80 μg and volume

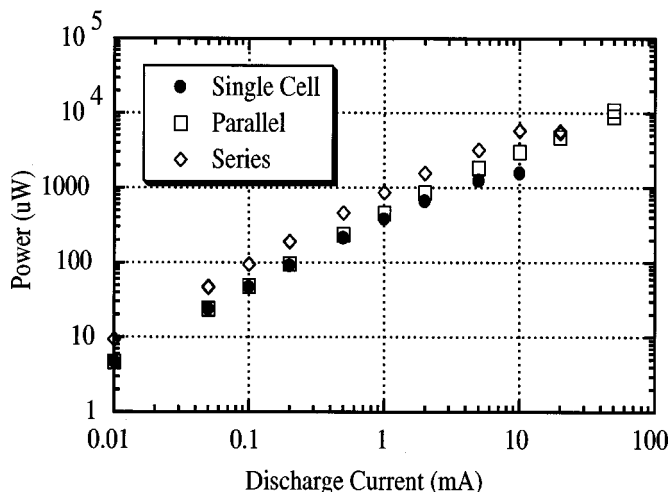


Figure 7. Power as a function of discharge current for a single microultracapacitor cell as well as parallel and series combinations. The power is calculated over 0-1 V for the single cell and parallel combination, and 0-2 V for the series combination.

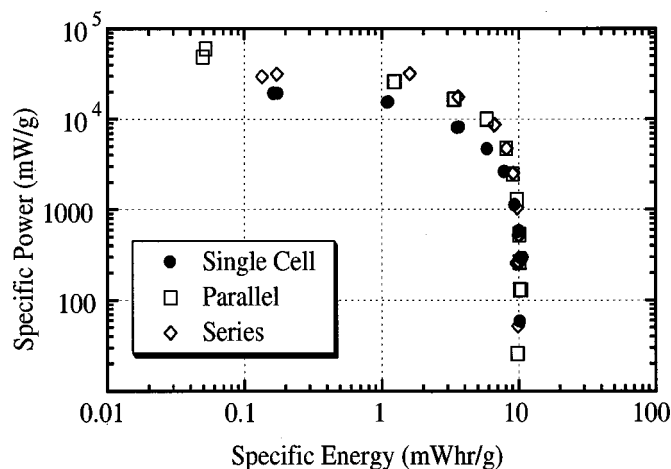


Figure 8. Ragone plot for single cell, parallel and series combinations of microultracapacitors. The mass for an individual microultracapacitor cell is $80 \mu\text{g}$ with an electrode area of 2 mm^2 and thickness of $15 \mu\text{m}$.

of $3 \times 10^{-5} \text{ mL}$ at 95% efficiency, the specific power is 1100 mW/g (2900 mW/mL) with a specific energy of 9 mWhr/g (24 mWhr/mL). By using combinations of two cells, we are able to obtain higher specific power while the specific energy reaches the same maximum. At 95% efficiency for parallel and series combinations, the specific energy is the same, but the specific power is over 2000 mW/g . Given our accounting of mass, these results provide some of the highest specific power reported for hydrous ruthenium oxide.¹

Conclusion

We have demonstrated the use of a laser engineering process based on laser direct write and laser micromachining to manufacture planar hydrous ruthenium oxide microultracapacitors with excellent electrochemical properties. CV measurements show that the transferred materials maintain the high specific capacitance of $\text{RuO}_2 \cdot 0.5\text{H}_2\text{O}$. The constant current charge and discharge behavior exhibits ideal capacitor behavior at discharge currents below 1 mA with deviations due to ohmic losses at higher currents. The power of the cells as a function of discharge current is successfully modeled as an ideal capacitor with ohmic polarizations and we are able to fit our data without the need for adjustable parameters. The microultracapacitors add in series and parallel which enables us to obtain higher voltages and discharge currents as high as 50 mA without damage to the cells. High specific power ($>10^4 \text{ mW/g}$) as well as specific energy (10 mWhr/g) are obtained by the microultracapacitor cells with a specific power of $\sim 1100 \text{ mW/g}$ at a charge efficiency of 95%. These values compare favorably to those reported in the literature for hydrous ruthenium oxide ultracapacitors. The favorable properties of these planar microultracapacitors fabricated by laser engineering opens the door to new advances in micro power sources for next generation microdevices.

Acknowledgments

This research was supported in part by the Office of Naval Research. C.B.A. acknowledges the support of the National Research Council postdoctoral associate program and R.C.W. acknowledges the support of the American Society for Engineering Education postdoctoral associate program.

The Naval Research Laboratory assisted in meeting the publication costs of this article.

References

1. A. Burke, *J. Power Sources*, **91**, 37 (2000).
2. B. E. Conway, *Electrochemical Supercapacitors, Scientific Fundamentals and Technological Applications*, Kluwer Academic, New York (1999).
3. R. Kotz and M. Carlen, *Electrochim. Acta*, **45**, 2483 (2000).
4. J. N. Harb, R. M. LaFollette, R. H. Selfridge, and L. L. Howell, *J. Power Sources*, **104**, 46 (2002).
5. J. B. Bates, N. J. Dudney, B. Neudecker, A. Ueda, and C. D. Evans, *Solid State Ionics*, **135**, 33 (2000).
6. K. E. Swider-Lyons, A. Piqué, C. B. Arnold, and R. C. Wartena, In *Electroactive Polymers and Rapid Prototyping*, D. B. Chrisey and S. C. Danforth, Editors, Vol. 689, p. 265, Materials Research Society, Pittsburgh, PA (2002).
7. J. P. Zheng, P. J. Cygan, and T. R. Jow, *J. Electrochem. Soc.*, **142**, 2699 (1995).
8. S. Sarangapani, B. Tilak, and C. Chen, *J. Electrochem. Soc.*, **143**, 3791 (1996).
9. S. Trasatti and P. Kurzweil, *Platinum Met. Rev.*, **38**, 46 (1994).
10. W. Dmowski, T. Egami, K. E. Swider-Lyons, C. T. Love, and D. R. Rolison, *J. Phys. Chem. B*, *In press*.
11. D. A. McKeown, P. L. Hagans, L. P. L. Carette, A. E. Russell, K. E. Swider, and D. R. Rolison, *J. Phys. Chem. B*, **103**, 4825 (1999).
12. Q. L. Fang, D. A. Evans, S. L. Roberson, and J. P. Zheng, *J. Electrochem. Soc.*, **148**, A833 (2001).
13. I. H. Kim and K. B. Kim, *Electrochem. Solid-State Lett.*, **5**, A62 (2001).
14. A. Piqué, D. B. Chrisey, J. M. Fitz-Gerald, R. A. McGill, R. C. Y. Auyeung, H. D. Wu, S. Lakeou, V. Nguyen, R. Chung, and M. Duignan, *J. Mater. Res.*, **15**, 1872 (2000).
15. D. B. Chrisey, A. Piqué, J. Fitz-Gerald, R. C. Y. Auyeung, R. A. McGill, H. D. Wu, and M. Duignan, *Appl. Surf. Sci.*, **154-155**, 593 (2000).
16. D. Young, R. C. Y. Auyeung, A. Piqué, D. B. Chrisey, and D. D. Dlott, *Appl. Phys. Lett.*, **78**, 3169 (2001).
17. C. B. Arnold, R. C. Wartena, B. Pratap, K. E. Swider-Lyons, and A. Piqué, In *Photon Processing in Microelectronics and Photonics*, J. J. Dubowski, K. Sugioka, M. C. Gower, R. F. Haglund, A. Piqué, and F. Traeger, Editors, Vol. 4367A, p. 353, International Society for Optical Engineering, Bellingham, WA (2002).
18. C. B. Arnold, R. C. Wartena, B. Pratap, K. E. Swider-Lyons, and A. Piqué, In *Electroactive Polymers and Rapid Prototyping*, D. B. Chrisey and S. C. Danforth, Editors, Vol. 689, p. 275, Materials Research Society, Pittsburgh, PA (2002).
19. W. G. Pell and B. E. Conway, *J. Power Sources*, **96**, 57 (2001).
20. K. E. Swider-Lyons, D. W. Weir, C. T. Love, R. Modi, T. Sutto, A. Piqué, and D. B. Chrisey, In *Power Sources for the New Millennium*, M. Jain, M. Ryan, S. Surampudi, R. Marsh, and G. Najarjan, Editors, PV 2000-22, p. 272, The Electrochemical Society Proceedings Series, Pennington, NJ (2000).
21. J. P. Zheng, *Electrochem. Solid-State Lett.*, **2**, 359 (1999).
22. D. Dunn and J. Newman, *J. Electrochem. Soc.*, **147**, 820 (2000).
23. C. Lin, B. N. Popov, and H. J. Ploehn, *J. Electrochem. Soc.*, **149**, A167 (2002).
24. C. Lin, J. A. Ritter, B. N. Popov, and R. E. White, *J. Electrochem. Soc.*, **146**, 3168 (1999).
25. V. Srinivasan and J. W. Weidner, *J. Electrochem. Soc.*, **146**, 1650 (1999).
26. J. Zhang, D. Jiang, B. Chen, J. Zhu, L. Jiang, and H. Fang, *J. Electrochem. Soc.*, **148**, A1362 (2001).
27. W. G. Pell and B. E. Conway, *J. Power Sources*, **63**, 255 (1996).
28. T. Christen and M. W. Carlen, *J. Power Sources*, **91**, 210 (2000).